

# Near-infrared photometry and radio continuum study of the massive star-forming regions IRAS 21413+5442 and IRAS 21407+5441

B. G. Anandarao,<sup>1★</sup> V. Venkata Raman,<sup>1★</sup> S. K. Ghosh,<sup>2★</sup> D. K. Ojha<sup>2★</sup>  
and M. S. N. Kumar<sup>3★</sup>

<sup>1</sup>Physical Research Laboratory (PRL), Navrangpura, Ahmedabad - 380009, India

<sup>2</sup>Tata Institute of Fundamental Research (TIFR), Homi Bhabha Road, Mumbai - 400005, India

<sup>3</sup>Centro de Astrofísica da Universidade do Porto, Rua das Estrelas, 4150-762 Porto, Portugal

Accepted 2008 August 11. Received 2008 August 11; in original form 2008 May 15

## ABSTRACT

IRAS 21413+5442 and IRAS 21407+5441 are two massive star-forming regions of high luminosity, likely associated with each other. Near-infrared (NIR) photometry on these two *IRAS* sources was performed at United Kingdom Infrared Telescope (UKIRT) using the UFTI under excellent seeing conditions yielding an angular resolution of  $\sim 0.5$  arcsec. Our results reveal details of stellar content to a completeness limit (90 per cent) of  $J = 18.5$ ,  $H = 18.0$  and  $K = 17.5$  mag in the two regions. In IRAS 21413+5442, we identify a late O-type star, having large  $H - K$  colour, to be near the centre of the CO jets observed by earlier authors. The UKIRT images reveal in IRAS 21407+5441, a faint but clear compact H II region around a central high- and intermediate-mass star cluster. We have detected a number of sources with large  $H - K$  colour which are not detected in  $J$  band. We also present the GMRT radio continuum map at 1.28 GHz covering the entire region surrounding the two star-forming clouds. The radio continuum fluxes are used to estimate the properties of H II regions which seem to support our NIR photometric results. Based on our radio continuum map and the archival Midcourse Space Experiment (MSX) 8.2- $\mu$ m image, we show that the two *IRAS* sources likely belong to the same parent molecular cloud and conjecture that a high-mass star of large IR colours, present in between the two sources, might have triggered star formation in this region. However, one cannot rule out the alternative possibility that Star A could be a nearby foreground star.

**Key words:** stars: formation – dust, extinction – H II regions – infrared: stars – radio continuum: general.

## 1 INTRODUCTION

Appearance of a compact H II (CHII) or an ultra-compact H II (UCHII) region embedded in a molecular cloud signifies the formation of a massive star of spectral type earlier than  $\sim B3$  (Shepherd & Churchwell 1996; Churchwell 2002). During this phase, the massive star is believed to be close to its zero-age main sequence (ZAMS), although pre-main-sequence (PMS) manifestations such as outflows have been detected in some cases (e.g. Weintraub & Kastner 1996; Beuther et al. 2002; Kumar, Keto & Clerkin 2006). Massive star formation occurs always in clusters. Further, the environment around the massive stars gets affected by their strong winds and energetic radiation. It is therefore important to study such CHII/UCHII regions in order to find out possible evolutionary stage of stellar content

in their vicinity. Near-infrared (NIR) photometry was shown to be very useful for this purpose (e.g. Lada 1985). Supplementary radio continuum measurements can provide important physical parameters concerning the object under certain assumptions (e.g. Scheffler & Elsasser 1988, and references therein). In this paper, we describe a study in NIR and radio continuum in and around two *IRAS* sources that are believed to be massive star-forming regions by virtue of the presence of CHII/UCHII.

IRAS 21413+5442 (Object 1) is one of the highly luminous, massive young stellar objects (YSOs) in our Galaxy and is situated at an estimated distance of 7.4 kpc (Wouterloot & Brand 1989; Yang et al. 2002). This source is identified with the presence of a UCHII region, called IRAS 21413+5442S, about 20 arcsec south of a CHII region, called IRAS 21413+5442N (Miralles, Rodríguez & Scalise 1994). The far-IR luminosity from *IRAS* fluxes at 12, 25 and 60  $\mu$ m was estimated to be  $3.2 \times 10^5 L_{\odot}$  (Campbell, Persson & Matthews 1989). The CO surveys of Shepherd & Churchwell (1996) have classified this source as a massive star-forming region

★E-mail: anand@prl.res.in (BGA); vvenkat@prl.res.in (VVR); swarna@tifr.res.in (SKG); ojha@tifr.res.in (DKO); nanda@astro.up.pt (MSNK)

with outflows of high velocity gas. This indicates therefore the PMS signature of the source that is believed to be at/near its ZAMS stage (due to the appearance of a UCHII region). Bronfman, Nyman & May (1996) detected this object in their survey of CS(2-1) rotational emission (at 97.981 GHz) that is believed to be a signature of high-density molecular gas. Ishii et al. (1998, 2002) have identified that the 3.1- $\mu\text{m}$  H<sub>2</sub>O ice in absorption which indicates the presence of a disc or thick nebular matter around the object. Ishii et al. (1998, 2002) classify this object as heavily obscured due to the larger excess in NIR colours. Interestingly, Shepherd & Churchwell (1996) have clearly mentioned that the source engine of the outflows (or jets) found in this object must be a heavily obscured (PMS) star yet to be discovered.

The second object in our study namely IRAS 21407+5441 (Object 2) was classified as a UCHII region from its *IRAS* colours and high luminosity of  $8 \times 10^4 L_{\odot}$  (Wood & Churchwell 1989:  $S_{25}/S_{12} \geq 3.7$  and  $S_{60}/S_{12} \geq 19.3$ ). The object however fell short of the sensitivity limit of Bronfman et al. (1996) survey of CS(2-1) line, possibly due to its low-density gas. This object is situated at about the same (kinematic) distance ( $\sim 8$  kpc) as Object 1, and is in all likelihood associated with it (as quoted in Carral et al. 1999 based on the rotation curve due to Wouterloot et al. 1990). At this distance, the two objects are separated in projection by about 20 pc (9.5 arcmin). The MSX *A*-band (8.2- $\mu\text{m}$ ) image of the region seems to support the association of the two *IRAS* sources; it also shows an interesting bright point source nearly mid-way between the two *IRAS* sources (called Star A in Fig. 1 and subsequent sections of the paper).

In this paper, we describe the first subarcsec United Kingdom Infrared Telescope (UKIRT) NIR photometry and 1.28 GHz radio continuum mapping in an attempt to classify the stellar content

in and around the two *IRAS* sources and to try and establish their association. We also examine the nature of Star A and its possible role in the region. We have also made use of archival Two-Micron All-Sky Survey (2MASS) and MSX data to supplement our study. In Section 2.1, the NIR photometry is presented and in Section 2.2, we present 1.28 GHz radio continuum mapping of the two objects. In Section 3, we describe the results from NIR photometry and radio continuum observations. Section 4 gives discussion of the results that reveal some new interesting insights on the two objects. Section 5 lists important conclusions of this work.

## 2 OBSERVATIONS

Fig. 1, generated from the 2MASS archival images, shows the two regions of our interest namely IRAS 21413+5442 (to the left-hand side, Object 1) and IRAS 21407+5441 (to the right-hand side, Object 2). Marked in the figure are three clusters – one in IRAS 21413+5442 (Cluster 1) and two in IRAS 21407+5441 (Clusters 2C and 2N). A bright star with large visual extinction, marked as Star A, is present in between the two *IRAS* sources. Also shown in the figure are the MSX low-resolution contours in *A* band (8.2  $\mu\text{m}$ ) overlaid on the 2MASS image. One may note the apparent association of the two *IRAS* sources with the Star A nearly at the middle. The observations made on these sources are described in the following two sections.

### 2.1 UKIRT–UFTI photometry at subarcsec resolution

Subarcsec resolution *JHK* photometry was performed at UKIRT during 2005 July 17 on the two objects under excellent seeing conditions ( $\sim 0.5$  arcsec) using the UFTI (HAWAII-1 1024  $\times$  1024)

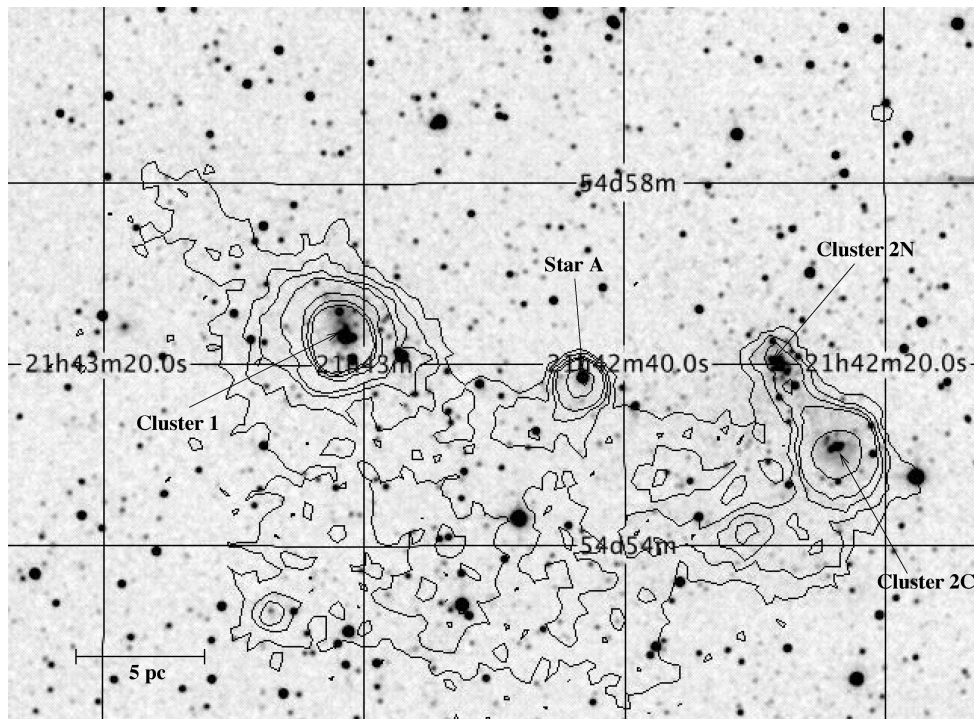


**Figure 1.** 2MASS  $K_s$ -band image of the combined field of the Clusters 1 and 2. For Cluster 2, the central source is marked as Cluster 2C and the north-eastern source as Cluster 2N. At the middle of the image, the highly reddened object Star A is shown. The abscissa (RA) and ordinate (Dec.) are for J2000 epoch. The overlaid contours represent MSX low-resolution image of the region; with contour levels 2, 3, 4, 5, 10, 15 and 20  $\text{W m}^{-2} \text{Sr}^{-1}$ . The linear size in the region shown at the bottom left-hand side assumes a distance of 7.4 kpc.

camera. The overall integration times were 75 s for each of the three bands. The plate scale is  $0.09 \text{ arcsec pixel}^{-1}$  that gives a useful central field of view (FOV) of  $\sim 75 \text{ arcsec}$  on the two objects. The standard star used was FS 151 (Hawarden et al. 2001) for both the sources.

The image processing was done by using standard IRAF tasks. Only those sources are considered which have photometric errors less than 0.1 mag for all the three bands. The 90 per cent completeness limits are  $J = 18.5$ ;  $H = 18.0$  and  $K = 17.5$  mag for the observations on the two objects.

We found from the MSX image archives (low-resolution mosaic images at an angular resolution of 18 arcsec, see Price et al. 2001) that the two IRAS sources in question seem to be physically linked, being part of a region that encompasses a large sky area (about  $8 \times 8 \text{ arcmin}$ ). Since the UKIRT photometry does not cover the entire region of MSX image data for the region, we have extracted 2MASS  $JHK_s$  photometric data for regions in between the two IRAS sources, including Star A and its environs.

## 2.2 1.28 GHz radio continuum observations at GMRT

The radio continuum observations in the 1.280-GHz frequency band (with a bandwidth of 16 MHz) were made on 2003 August 1 at the Giant Metrewave Radio Telescope (GMRT), operated by National Centre for Radio Astrophysics (NCRA), Tata Institute of Fundamental Research (TIFR) near Pune (the details of the telescope can be found in Swarup et al. 1991). Out of the total 30 antennae, 26 had operated on the day of observations. The calibration sources used were 3C 286 and 3C 48 for flux and 2202+422 for phase. The FOV includes both the objects encompassing a region of  $10 \times 10 \text{ arcmin}^2$ . The image processing was done by using AIPS software. The data sets were checked for dead antennas, bad baseline, bad time ranges, spikes etc. using the tasks UVPLT and VPLT. The tasks UVFLG and TVFLG were used for subsequent editing. Maps of the field were generated by Fourier transform and subsequent cleaning and deconvolution using the IMAGR task. The final angular resolution on the map is  $\sim 30 \text{ arcsec}$  (beam size), after using adequate UV tapering on the available base lines. The rms noise in the radio map is  $1.4 \text{ mJy beam}^{-1}$ .

## 3 RESULTS

Here, we essentially deal with the three clusters seen in Fig. 1: the one around the central H II region in IRAS 21413+5442 (Cluster 1); and the central and the north-eastern clusters in IRAS 21407+5441 (Cluster 2C and Cluster 2N, respectively). Figs 2–4 show the UKIRT  $K$ -band images of the three clusters, respectively. The images represent approximately  $90 \times 90 \text{ arcsec}^2$  FOV, although the best image quality and high signal-to-noise ratio were restricted to the central region of FOV  $75 \times 75 \text{ arcsec}^2$ . The visual extinction,  $A_V$ , for each of the identified stars was computed from the  $HK$  photometric magnitudes, using the Bessell & Brett (1988) formulae based on the extinction law of Rieke & Lebofsky (1985), with the ratio of total-to-selective extinction  $R_V = 3.1$ . The standard colour–colour diagram (CCD) and colour–magnitude diagram (CMD) were constructed and shown in Fig. 5 for the three clusters. Also shown in the CCDs is unreddened main-sequence locus, unreddened locus of giant stars (from Bessell & Brett 1988). The extinction vectors are shown for B0 and M8 main-sequence stars. The T Tauri star locus is taken from Meyer, Calvet & Hillenbrand (1997). The CMD was constructed assuming a distance of 7.4 kpc for both the sources.

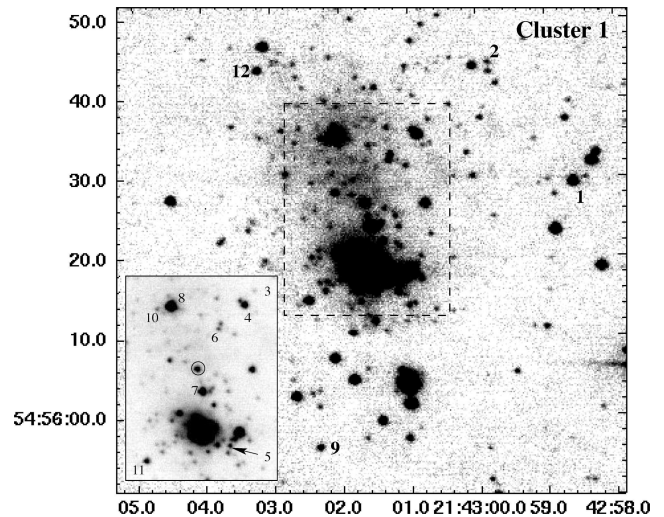


**Figure 2.** UKIRT  $K$ -band image of IRAS 21413+5442 (Cluster 1). The inset at the bottom left-hand side represents the central region (see the dashed lines in the main figure) and shows the identified stars with large IR excess falling in the T Tauri star region and beyond (see the text and Table 1). The star (no. 7) that was shown encircled is situated at the centre of the CO jets. There are several ‘red objects’ that are detected only in  $H$  and  $K$  bands with large  $H - K$  colour (see the text, Fig. 5 and Table 1). The abscissa (RA) and ordinate (Dec.) are for J2000 epoch.

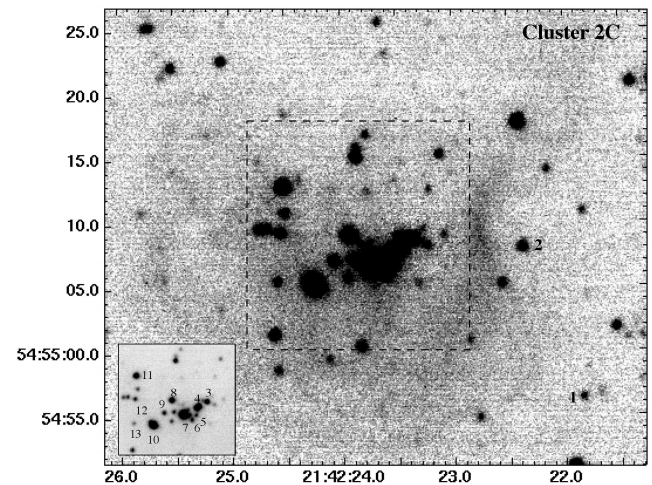


**Figure 3.** UKIRT  $K$ -band image of IRAS 21407+5441: central region (Cluster 2C) revealing the H II region with filamentary structures. The inset at the bottom left-hand side shows stars identified, as in Fig. 2 (see also the text and Table 2). There are several ‘red objects’ that are detected only in  $H$  and  $K$  bands with large  $H - K$  colour (see the text, Fig. 5 and Table 2). The abscissa (RA) and ordinate (Dec.) are for J2000 epoch.

The theoretical positions of several main-sequence spectral types are also shown in the diagram with corresponding reddening vectors. We have listed in Tables 1–3, the positions,  $H$  magnitudes,  $H - K$  and  $J - H$  colours and the visual extinctions ( $A_V$ ) for all the stars detected to the completeness limits in Cluster 1, Cluster 2C and 2N, respectively. The stars with large excess falling in the T Tauri region and beyond are shown in serial numbers in brackets. These are also marked on the images in Figs 2–4. The spectral types obtained from the  $K$  versus  $H - K$  plots were verified against  $J$  versus  $J - H$  plots and found that there is a very good agreement. Considering the

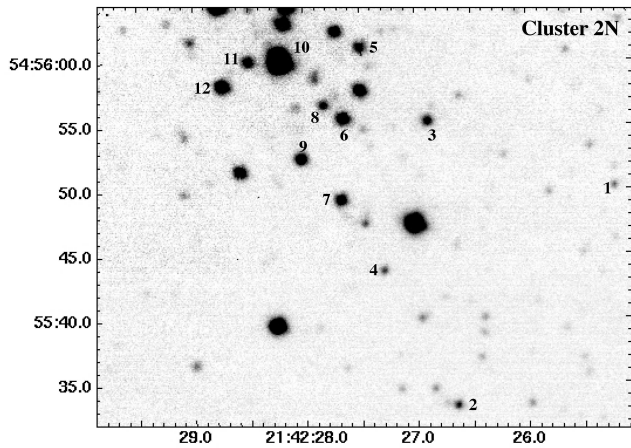


**Figure 4.** UKIRT  $K$ -band image of IRAS 21407+5441: North-eastern region (Cluster 2N). Stars identified are numbered (see the text and Table 3). There are several ‘red objects’ that are detected only in  $H$  and  $K$  bands with large  $H - K$  colour (see the text, Fig. 5 and Table 3). The abscissa (RA) and ordinate (Dec.) are for J2000 epoch.

uncertainties in the exact distance of the sources and in the photometry, it is difficult to determine accurate spectral types based only on CMDs. Further, the spectral classes would have been slightly overestimated (by a couple of subclasses) for some sources that

have substantial intrinsic infrared excess as they probably represent relatively early PMS stars (Class I).

We find a number of stars detected only in  $H$  and  $K$  bands but not in  $J$  band in the UKIRT photometry. These are also shown in the CMDs in Fig. 5. Some of these have large  $H - K$  colour excesses ( $\geq 1.5$ ), especially those that are found in Clusters 1 and 2C. These sources could be low-/intermediate-mass PMS stars. These stars, with  $(H - K) \geq 1.0$ , are also listed in Tables 1–3.

The radio continuum contour map in 1.280 GHz as shown in Fig. 6 captures the two objects IRAS 21413+5442 and IRAS 21407+5441 in a single observation due to the large FOV ( $10 \times 10$  arcmin<sup>2</sup>) of GMRT. Also shown overlaid on the radio contours in Fig. 6 is the MSX low-resolution mosaic image. The figure shows two dense regions, one around the northern and southern H II regions in the Object 1 and the other, a more dense and intense one, around the central cluster of the Object 2 (Cluster 2C; see Fig. 6). The radio contours show a maximum around Star A that lies mid-way between Object 1 and Objects 2C and 2N. Our radio map compares very well with the NVSS 21-cm image of the region. The MSX  $A$ -band image also correlates well with the radio map; the low level extended emission probably representing warm gas/dust. Fig. 7 shows the 1.28-GHz flux density contours overlaid on the  $K$ -band images of Objects 1 and 2 (respectively, A and B in Fig. 7). Since the beam size is about 30 arcsec, the radio map shows the two H II regions of Object 1 as a single region, with a detected extension consistent with the location of these H II regions.

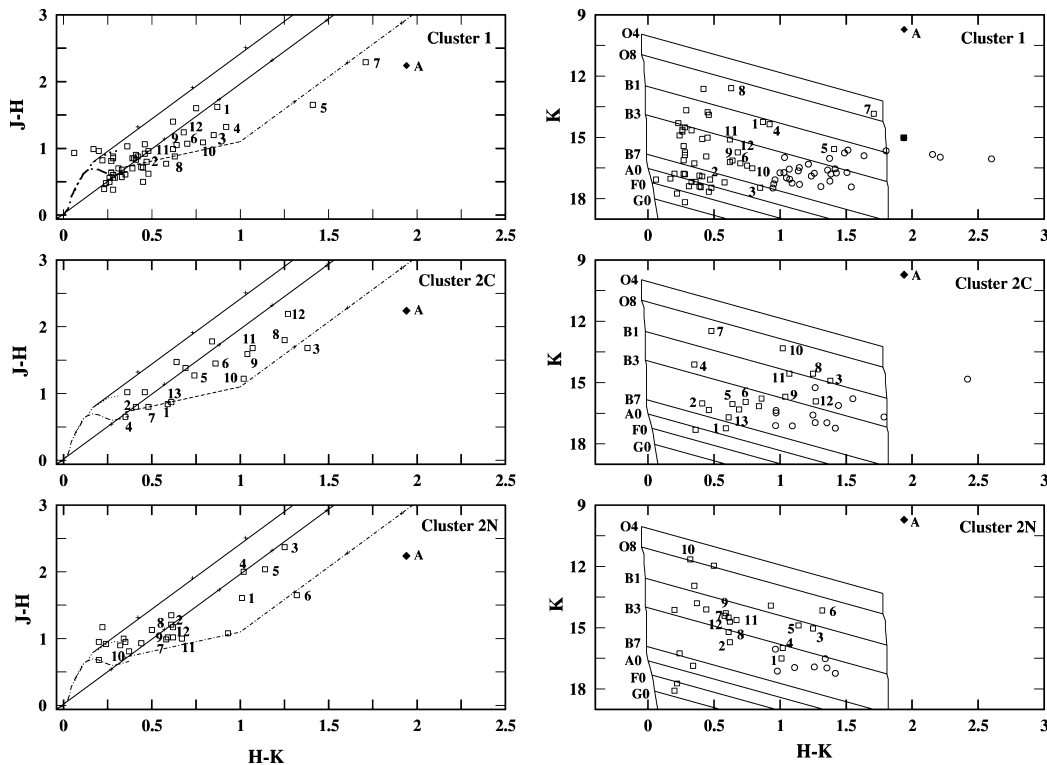


**Figure 5.** CMDs (left-hand panels) for the sources in the central H II regions in IRAS 21413+5442 (Cluster 1, in top panel) and Cluster 2C (middle panel) and Cluster 2N (bottom panel) in IRAS 21407+5441. The thick dashed curve represents the unreddened main-sequence stars; the thin dotted curve shows the unreddened giant stars. The straight lines indicate the extinction vectors for  $A_V = 30$  mag and the crosses on the vectors indicate the visual extinction for 5 mag intervals. The T Tauri stars fall on the dashed straight line, while the dot-dashed straight line represents the extinction vector for the T Tauri stars. CMDs (right-hand panels) are also shown. The vertical lines indicate the unreddened main-sequence stars of different spectral types (on the left-hand panel) and the same with an extinction of  $A_V = 30$  mag (on the right-hand panel); the slanting lines showing the extinction vectors. The stars that are common for all the  $JHK$  bands are shown by open squares and the stars that are detected only in  $HK$  bands are shown by open circles. The filled square represents the embedded star shown circled in Fig. 2. The diamond symbol marked as ‘A’ represents the position of Star A, shown for comparison.

**Table 1.** UKIRT *JHK* photometry of sources in the central H II regions (Cluster 1) of IRAS 21413+5442. The numbers in brackets in the  $A_V$  column identify stars with IR excesses in T Tauri region and beyond. The stars listed after the gap are detected only in *HK* bands.

RA (2000)	Dec. (2000)	<i>H</i>	<i>H</i> – <i>K</i>	<i>J</i> – <i>H</i>	$A_V$	RA (2000)	Dec. (2000)	<i>H</i>	<i>H</i> – <i>K</i>	<i>J</i> – <i>H</i>	$A_V$
21:42:58.54	54:56:29.61	15.11	0.87	1.62	14.4 (1)	21:43:03.42	54:56:16.56	17.53	0.36	1.03	5.9
21:42:58.63	54:56:39.78	17.94	0.48	0.96	7.9	21:43:03.56	54:56:22.51	17.7	0.31	0.70	11.6
21:42:58.67	54:56:37.60	16.62	0.35	0.61	5.8	21:43:03.60	54:56:22.08	17.51	0.33	0.68	5.4
21:42:58.78	54:56:23.60	14.37	0.46	0.92	7.6	21:43:03.75	54:56:54.14	14.22	0.45	0.71	7.4
21:42:58.80	54:56:28.08	17.79	0.39	0.70	6.4	21:43:04.06	54:56:48.02	17.97	0.22	0.82	3.6
21:42:58.84	54:56:52.38	17.32	0.41	0.83	6.8	21:43:04.30	54:56:27.44	14.98	0.33	0.57	5.4
21:42:58.90	54:56:29.93	18.12	0.46	1.06	7.6	21:43:04.58	54:55:58.98	17.05	0.27	0.81	4.5
21:42:59.30	54:56:05.79	17.25	0.39	0.85	6.4						
21:42:59.78	54:56:44.69	17.54	0.47	0.80	7.8 (2)						
21:42:59.89	54:56:37.68	17.08	0.28	0.85	4.6	21:42:58.88	54:56:11.20	18.02	1.26		20.8
21:43:00.00	54:56:44.20	15.7	0.27	0.63	4.5	21:42:59.93	54:56:30.27	18.23	1.51		24.9
21:43:00.07	54:56:33.30	17.13	0.06	0.93	1.0	21:43:00.68	54:56:17.42	17.62	1.15		18.9
21:43:00.24	54:56:13.41	18.45	0.28	0.38	4.6	21:43:00.81	54:56:36.15	17.02	1.03		17.1
21:43:00.56	54:56:23.14	17.84	0.4	0.85	6.6	21:43:00.86	54:56:14.13	17.62	1.07		17.7
21:43:00.64	54:56:37.60	18.32	0.85	1.20	14.0 (3)	21:43:00.99	54:56:21.54	18.04	0.96		15.9
21:43:00.65	54:56:26.97	14.97	0.26	0.50	4.3	21:43:01.01	54:56:24.08	17.75	1.03		17.0
21:43:00.69	54:56:55.68	16.83	0.62	1.40	10.2	21:43:01.02	54:56:15.82	17.40	1.38		22.7
21:43:00.70	54:56:20.44	17.78	0.58	0.77	9.6	21:43:01.06	54:56:25.42	18.12	1.07		17.7
21:43:00.76	54:56:49.47	17.19	0.17	0.99	2.8	21:43:01.21	54:56:26.32	18.33	1.09		18.0
21:43:00.79	54:56:35.64	15.27	0.92	1.32	15.2 (4)	21:43:01.24	54:56:22.26	17.14	1.51		25.0
21:43:00.83	54:55:57.45	16.14	0.28	0.60	4.6	21:43:01.26	54:56:24.54	18.17	1.43		23.5
21:43:00.83	54:56:01.76	13.96	0.29	0.56	4.8	21:43:01.30	54:56:24.11	17.53	1.22		20.1
21:43:00.85	54:56:18.51	13.04	0.42	0.88	6.9	21:43:01.34	54:56:16.00	17.46	1.80		29.8
21:43:00.90	54:56:47.41	16.97	0.2	0.96	3.3	21:43:01.36	54:56:41.54	17.73	0.99		16.5
21:43:00.95	54:56:06.00	16.02	0.28	0.88	4.6	21:43:01.36	54:56:12.20	17.99	2.16		35.6
21:43:00.99	54:56:16.75	16.98	1.41	1.65	23.3 (5)	21:43:01.46	54:56:18.17	14.71	4.26		70.4
21:43:01.16	54:56:33.20	17.13	0.75	1.60	12.4	21:43:01.50	54:56:27.07	16.95	1.94		32.0
21:43:01.19	54:56:16.91	15.46	0.45	0.50	7.4	21:43:01.56	54:56:14.64	17.78	1.14		18.8
21:43:01.19	54:56:32.46	16.97	0.7	1.07	11.6 (6)	21:43:01.63	54:56:15.95	18.66	2.60		42.9
21:43:01.23	54:55:59.62	15.48	0.41	0.90	6.8	21:43:01.69	54:56:28.08	18.52	1.38		22.7
21:43:01.23	54:56:36.56	17.26	0.39	0.70	6.4	21:43:01.69	54:56:10.80	17.95	1.42		23.4
21:43:01.44	54:56:24.06	15.56	1.71	2.29	28.2 (7)	21:43:01.80	54:56:21.16	18.20	3.52		58.1
21:43:01.63	54:56:04.83	14.53	0.23	0.39	3.8	21:43:01.84	54:56:18.33	18.18	2.21		36.5
21:43:01.92	54:56:07.50	14.89	0.26	0.56	4.3	21:43:01.87	54:56:17.41	18.18	1.39		22.9
21:43:01.95	54:56:35.51	13.21	0.63	0.88	10.4 (8)	21:43:01.91	54:56:39.18	18.43	0.95		15.6
21:43:01.97	54:56:51.85	16.38	0.44	0.72	7.3	21:43:01.92	54:56:20.31	17.53	1.64		27.0
21:43:02.11	54:55:56.38	16.77	0.64	1.05	10.6 (9)	21:43:01.94	54:56:28.33	17.25	1.49		24.6
21:43:02.12	54:56:01.49	17.95	0.48	0.62	7.9	21:43:02.07	54:56:39.90	18.23	0.95		15.7
21:43:02.17	54:56:35.20	17.3	0.79	1.09	13.0 (10)	21:43:02.27	54:56:20.27	18.13	1.24		20.4
21:43:02.30	54:56:14.84	15.72	0.62	0.99	10.2 (11)	21:43:02.27	54:56:03.19	18.97	1.54		25.4
21:43:02.46	54:56:02.76	15.14	0.24	0.48	3.9	21:43:02.65	54:56:30.76	17.96	1.36		22.4
21:43:02.95	54:56:08.53	16.39	0.27	0.64	4.5	21:43:02.70	54:56:36.25	18.03	1.05		17.3
21:43:03.02	54:56:46.77	14.79	0.28	0.56	4.6	21:43:03.43	54:56:36.83	18.72	1.31		21.6
21:43:03.09	54:56:43.78	16.41	0.68	1.24	11.2 (12)	21:43:03.60	54:56:12.62	18.45	1.15		18.9

## 4 DISCUSSION

### 4.1 Stellar content in the three clusters

In the case of Cluster 1 (Fig. 2), we find a few YSOs close to the bright UCHII region at the centre. Notable among these are the star no. 7 (Fig. 5, top panel) which is of spectral type earlier than O8 and the star no. 5 which is a B2-type star. Also present closely surrounding the bright central UCHII region are the several sources that are detected only in *HK* bands (but not in *J* band to the detection limit). Notable among these ‘red objects’ is the one north of the star 7 (marked with a circle around it in Fig. 2 and by a filled square in the CMD in Fig. 5, top right-hand panel) having a *H* – *K* colour of nearly two and of spectral type earlier than B0. Interestingly, its position very nearly coincides with that of the centre of the CO outflows detected in this object by Shepherd &

Churchwell (1996). We note a number of PMS stars very closely surrounding the UCHII region: the formation of which was possibly triggered by the expanding shock front. It is also to be noted that the bright central core of the UCHII region is detected only in *HK* bands with a *H* – *K* colour of more than four (see Table 1). The CHII region towards the north appears to be powered by a O9-type star (no. 8) that shows moderate excess as compared to the stars in UCHII region towards its south. The stars 5 and 7 suffer large visual extinction (as seen in the CMD in Fig. 5),  $A_V$ , of 23.3 and 28.2 mag (Table 1) and may represent PMS stars of Class I. As mentioned earlier, the spectral classes assigned purely on the basis of CMDs, could have been overestimated, especially for the objects with large colour excesses.

In Cluster 2C (Fig. 3), a CHII region can be very clearly seen in the *K*-band image of UKIRT encompassing the cluster, with a number of curved filamentary structures. In Fig. 3, one can note that

**Table 2.** UKIRT *JHK* photometry of sources in the central cluster (Cluster 2C) of IRAS 21407+5441. The numbers in brackets in the  $A_V$  column identify stars with IR excesses in T Tauri region and beyond. The stars listed after the gap are detected only in *HK* bands.

RA (2000)	Dec. (2000)	<i>H</i>	<i>H</i> – <i>K</i>	<i>J</i> – <i>H</i>	$A_V$	RA (2000)	Dec. (2000)	<i>H</i>	<i>H</i> – <i>K</i>	<i>J</i> – <i>H</i>	$A_V$
21:42:20.64	54:55:36.51	17.56	0.49	0.92	8.1	21:42:24.39	54:55:33.43	17.66	0.33	0.83	5.5
21:42:20.85	54:54:37.49	17.92	0.4	1.06	6.6	21:42:24.40	54:55:09.29	17.01	0.69	1.38	11.4
21:42:20.91	54:55:00.80	12.79	0.4	0.94	6.6	21:42:24.43	54:55:11.32	15.63	1.07	1.68	17.7 (11)
21:42:21.03	54:55:19.35	13.37	0.25	0.52	4.1	21:42:24.45	54:55:07.69	17.19	1.27	2.19	21.0 (12)
21:42:21.29	54:55:19.23	16.35	0.34	0.76	5.6	21:42:24.48	54:55:03.95	17.32	0.61	0.87	10.1 (13)
21:42:21.41	54:55:00.26	16.83	0.49	0.94	8.1	21:42:24.58	54:55:38.36	16.05	0.35	0.73	5.8
21:42:21.53	54:55:37.20	17.33	0.37	1.05	6.1	21:42:24.79	54:54:44.70	14.58	0.21	0.52	3.5
21:42:21.71	54:54:54.88	17.84	0.59	0.84	9.7 (1)	21:42:24.98	54:55:21.07	16.8	0.46	1.02	7.6
21:42:21.79	54:54:49.37	14.9	0.27	0.63	4.5	21:42:25.20	54:54:47.25	16.17	0.3	0.76	5.0
21:42:21.80	54:55:39.18	15.47	0.48	1.05	7.9	21:42:25.89	54:55:31.79	17.2	0.34	1.00	5.6
21:42:22.04	54:55:12.50	17.67	0.36	1.02	5.9	21:42:25.98	54:54:36.65	16.4	0.26	0.89	4.3
21:42:22.06	54:54:42.64	17.76	0.44	0.96	7.3	21:42:26.02	54:55:28.38	16.15	0.82	1.43	13.5
21:42:22.08	54:55:29.92	15.96	0.35	0.68	5.8	21:42:26.03	54:54:37.83	15.65	0.34	0.67	5.6
21:42:22.26	54:55:06.50	16.43	0.41	0.80	6.8 (2)	21:42:26.08	54:55:12.81	16.94	0.44	1.06	7.3
21:42:22.55	54:55:30.27	17.75	0.41	1.02	6.8	21:42:26.33	54:54:48.86	18.	0.39	0.75	6.4
21:42:22.98	54:54:39.73	16.8	0.42	0.93	6.9	21:42:26.55	54:55:31.71	16.33	0.62	1.17	10.2
21:42:23.04	54:54:43.89	18.05	0.47	0.95	7.8	21:42:26.68	54:55:00.08	16.41	0.25	0.79	4.1
21:42:23.24	54:55:07.17	16.28	1.38	1.68	22.8 (3)						
21:42:23.25	54:55:36.96	15.74	1.46	1.72	24.1						
21:42:23.38	54:55:06.46	14.47	0.35	0.65	5.8 (4)	21:42:22.31	54:55:16.20	17.257	2.42		39.9
21:42:23.42	54:55:05.13	16.68	0.74	1.27	12.2 (5)	21:42:22.44	54:55:03.73	18.475	1.79		29.5
21:42:23.50	54:55:04.44	16.65	0.86	1.45	14.2 (6)	21:42:23.01	54:55:13.73	17.839	1.25		20.6
21:42:23.59	54:54:42.54	13.68	0.47	1.10	7.8	21:42:23.56	54:55:24.01	18.077	0.97		16.0
21:42:23.64	54:55:05.24	12.96	0.48	0.80	7.9 (7)	21:42:23.64	54:55:06.78	18.215	1.09		18.0
21:42:23.72	54:54:58.88	16.69	0.64	1.47	10.6	21:42:23.67	54:55:15.34	18.228	1.27		21.0
21:42:23.74	54:54:47.99	16.84	0.44	0.94	7.3	21:42:23.76	54:55:13.58	16.511	1.27		21.0
21:42:23.83	54:55:07.48	15.81	1.25	1.80	20.6 (8)	21:42:24.50	54:54:59.86	17.341	1.55		25.6
21:42:23.84	54:55:04.24	17.	0.84	1.78	13.9	21:42:24.57	54:55:08.08	17.566	1.44		23.8
21:42:23.94	54:55:38.03	18.13	0.54	1.07	8.9	21:42:24.65	54:55:08.02	17.335	0.97		16.0
21:42:23.96	54:55:05.49	16.73	1.04	1.59	17.2 (9)	21:42:25.43	54:55:20.59	17.449	0.97		16.0
21:42:24.07	54:54:40.22	15.26	0.26	0.59	4.3	21:42:26.31	54:55:38.50	18.324	1.36		22.4
21:42:24.14	54:55:03.66	14.33	1.02	1.22	16.8 (10)	21:42:26.34	54:55:35.41	18.653	1.42		23.4

**Table 3.** UKIRT *JHK* photometry of sources in the north-eastern cluster (Cluster 2N) of IRAS 21407+5441. The numbers in brackets in the  $A_V$  column identify stars with IR excesses in T Tauri region and beyond. The stars listed after the gap are detected only in *HK* bands.

RA (2000)	Dec. (2000)	<i>H</i>	<i>H</i> – <i>K</i>	<i>J</i> – <i>H</i>	$A_V$	RA (2000)	Dec. (2000)	<i>H</i>	<i>H</i> – <i>K</i>	<i>J</i> – <i>H</i>	$A_V$
21:42:25.13	54:55:48.62	17.52	1.01	1.61	16.7 (1)	21:42:28.22	54:56:00.03	11.98	0.32	0.9	5.3 (10)
21:42:25.89	54:55:31.79	17.2	0.34	1.00	5.6	21:42:28.43	54:55:58.35	15.29	0.67	1.00	11.1 (11)
21:42:25.91	54:55:56.87	17.95	0.22	1.17	3.6	21:42:28.50	54:56:00.07	15.33	0.62	1.02	10.2 (12)
21:42:26.55	54:55:31.71	16.33	0.62	1.17	10.2 (2)	21:42:28.51	54:55:49.85	14.32	0.2	0.68	3.3
21:42:26.82	54:55:53.67	16.29	1.25	2.37	20.6 (3)	21:42:28.67	54:55:56.46	14.17	0.37	0.81	6.1
21:42:26.94	54:55:45.79	12.48	0.5	1.13	8.3	21:42:28.92	54:55:34.90	16.5	0.24	0.92	4.0
21:42:27.22	54:55:42.23	17.01	1.02	2.00	16.8 (4)	21:42:29.36	54:55:40.64	18.29	0.2	0.95	3.3
21:42:27.42	54:55:56.12	14.54	0.44	0.93	7.3						
21:42:27.50	54:56:01.40	16.03	1.14	2.04	18.8 (5)						
21:42:27.58	54:55:53.90	15.48	1.32	1.65	21.8 (6)	21:42:25.73	54:55:48.19	18.10	0.98		16.2
21:42:27.60	54:55:47.69	15.00	0.58	0.99	9.6 (7)	21:42:26.31	54:55:38.50	18.32	1.36		22.4
21:42:27.72	54:56:02.33	15.11	0.61	1.35	10.1	21:42:26.34	54:55:35.41	18.65	1.42		23.4
21:42:27.76	54:55:54.96	15.82	0.61	1.21	10.1 (8)	21:42:26.54	54:55:55.66	18.06	1.11		18.3
21:42:27.96	54:55:50.86	14.88	0.59	1.02	9.7 (9)	21:42:26.87	54:55:38.48	17.86	1.34		22.1
21:42:28.18	54:55:37.95	13.3	0.35	0.95	5.8	21:42:27.38	54:55:45.87	17.02	0.97		16.0
21:42:28.20	54:55:57.99	14.84	0.93	1.08	15.3	21:42:27.39	54:55:53.07	18.18	1.26		20.8

the CHII region has a sharp edge towards west. The presence of stars earlier than B3 prompts us to believe that the faint halo around the cluster is a CHII region. Our radio continuum observations show a very intense emission surrounding the cluster suggesting a H II

region (see Figs 6 and 7). There are about 13 stars in this cluster which fall in T Tauri region (Fig. 5, middle panel). We find at least 11 stars that are between spectral types earlier than B5 (Fig. 5, middle panel and Table 2). For a few early-type stars, the  $A_V$  is quite high

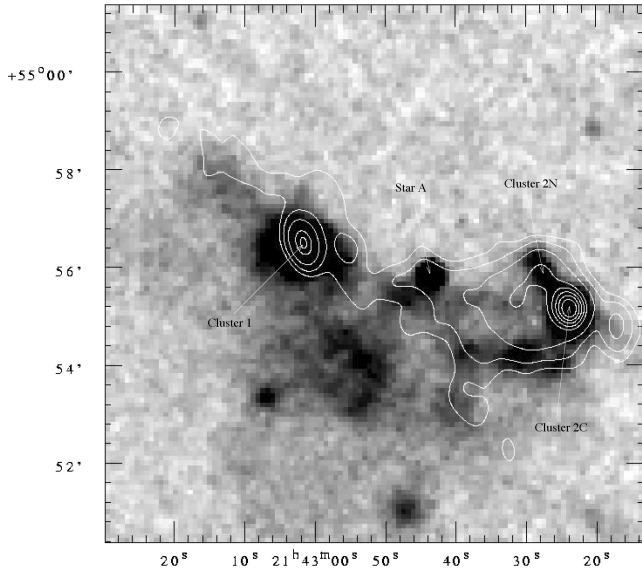


**Figure 6.** MSX A band (8.2  $\mu\text{m}$ ) low-resolution mosaic image of the region shown overlaid by the 1.28 GHz radio continuum contours: Clusters 1, 2C and 2N are shown by arrows as is the Star A (cf. Fig. 1). The radio contours represent flux density values of 10, 20, 40, 80, 100, 120, 140, 160 and 180  $\text{mJy beam}^{-1}$ . The beam size is 30 arcsec. The abscissa (RA) and ordinate (Dec.) are for J2000 epoch.

(as seen in the CMD in Fig. 5, middle right-hand panel); star no. 8, a B0.5 type with 20.6 mag; star no. 11, B1 type with 17.7 mag; star no. 3, a B1 type with 22.8 mag which may be a Class I PMS star; star no. 12 of B2.5 type with 21.0 mag and star no. 9 of B3 type with an  $A_V$  of 17.2 mag. The stars 7 and 10 having spectral type of O9–O9.5 with  $A_V$  7.9 and 16.8 mag, respectively, seem to be the main sources for the H II region. The star 4 has  $A_V$  of nearly 5.8 mag showing that it may be of a ZAMS star of spectral type B2.

At an angular separation of about 90 arcsec, to the north-east of the central cluster of IRAS 21407+5441, lies another cluster, Cluster 2N (Fig. 4). Our UKIRT images cover it nearly completely (as verified from the 2MASS image of the region). There are about 12 stars in this cluster that fall into the T Tauri zone (Fig. 5, bottom

panel). At the centre of the cluster is a O8 ZAMS star (star 10 in UKIRT image in Fig. 4) that showed an  $A_V$  of 5.3 (as seen in the CMD in Fig. 5, bottom right-hand panel and listed in Table 3). Star 6 (O9.5 type) and star 3 (B1 type) suffer large  $A_V$  of 21.8 and 20.6 mag, respectively, with the former likely to be a Class I PMS star; while star 5 (type B1) and star 4 (type B3) suffer 18.8 and 16.8 mag, respectively.

In all the three clusters discussed above the stars fall in to or a little beyond the T Tauri zone (see Fig. 5) and have  $H - K$  colours more than 1.0. These sources may be considered to be mostly Class II with large NIR excess (Classical T Tauri stars) or extremely reddened early-type ZAMS stars, having excess emission in K band (e.g. Blum, Damiani & Conti 2001, and references therein). Our CMDs support the latter scenario as also supported by the presence of H II regions.

In addition to these three clusters, we looked into the 2MASS data on the region between the two IRAS sources. Interesting among the sources in this region is the Star A (marked in Fig. 1 as well in Fig. 5 for comparison with other stars). The 2MASS photometry shows that this object is a high-mass star of spectral type earlier than O4 with large colour excess ( $J - H = 2.24$  and  $H - K = 1.94$ ) and hence suffering a visual extinction of 32 mag. It is possible that this star could belong to the molecular cloud from which the three clusters formed later. Alternatively, this may be a background star, not associated with the cloud but obscured by it in the line of sight.

The MSX A-band contours shown in Fig. 1 (and the image in Fig. 6) indicate extended low-level ( $\sim 2-4 \times 10^{-6} \text{ W m}^{-2} \text{ Sr}^{-1}$ ) mid-infrared emission towards the south of Star A, apart from the more intense emission around the two IRAS sources. Of the nine MSX point sources present in the region (with detection quality four in the 8.2- $\mu\text{m}$  A band), we find five are associated with the two IRAS sources (two in each) and Star A. It may be mentioned that the MSX fluxes correspond to several resolved sources in UKIRT images in each of the three clusters. The other four MSX point sources are present towards south-east and south-west of Star A. Most of these sources have fluxes good only in A band. We have extracted 2MASS archival  $JHK_s$  data (of quality 'A' in all the three bands) in this region and found that the Star A stands out with its large colour excesses. The other stars (including the counterparts

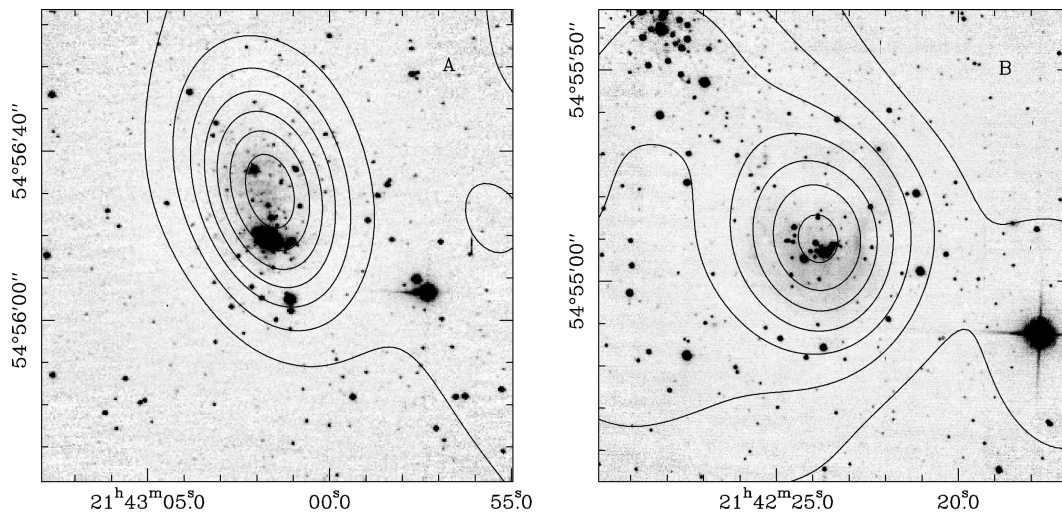


**Figure 7.** GMRT 1.28 GHz contours overlaid on the UKIRT K-band images of IRAS 21413+5442 (A on the left-hand panel) and IRAS 21407+5441 (B on the right-hand panel). The contour flux density levels correspond to 10–100  $\text{mJy beam}^{-1}$  in steps of 15  $\text{mJy beam}^{-1}$  for A and 25–175  $\text{mJy beam}^{-1}$  in steps of 25  $\text{mJy beam}^{-1}$ . The beam size is 30 arcsec. The abscissa (RA) and ordinate (Dec.) are for J2000 epoch.

for the four MSX point sources), mostly falling between the two extinction vectors for main sequence; and if assumed to be at the same distance as the two *IRAS* sources, represent massive stars of late O type or early B type. Hence, we believe that they are foreground stars. Using the code *DUSTY* (Ivezic, Nenkova & Elitzur 1999), we have modelled the Spectral Energy Distribution (SED) of Star A, taking data from 2MASS and MSX archives and found that the SED fits well with a  $T_{\text{eff}} \sim 30000$  K with emission also from graphite dust grains at  $T = 650$  K, indicating that the star may be very massive and obscured. Interestingly, Star A does not have a counterpart in *IRAS* data. If the Star A is indeed a massive PMS star with a UCH II around, then the emission should peak around  $100 \mu\text{m}$  (e.g. Churchwell 2002). So it appears that it is well beyond its PMS phase with warm dust/gas in an accretion disc.

There are about 43 stars with  $H - K$  colour  $\geq 0.50$  in Cluster 1, about 30 in Cluster 2C and about 25 in Cluster 2N, as identified from UKIRT photometry. Assuming that they represent PMS-embedded sources, we can infer that the volume density for the three clusters seems to be less than that for a typical massive star-forming cloud (e.g. Smith 2004).

#### 4.2 Parameters from radio continuum

Here, in this section, we derive some physical parameters from the radio fluxes and also estimate the distances to the sources by combining the radio and NIR data. Assuming the continuum emission is caused by free-free radiation from accelerated electrons (thermal Bremsstrahlung), we expect a power law for the spectral energy distribution with an index of  $\sim 0.1$ . However, Miralles et al. (1994) have shown that among several UCH II regions that they studied in two radio frequencies (4.9 and 14.9 GHz), only the southern UCH II region (in the Object 1) showed an index of  $0.99 \pm 0.01$ . It was suggested by these authors that the object must be obscured by dust.

First, we try to determine the individual 1.28 GHz continuum flux for the two H II regions in Object 1. Adopting a spectral index of  $\sim 1.0$  (from Miralles et al. 1994), one would expect a flux of  $\sim 30$  mJy for the GMRT observation at 1.28 GHz. The index for the northern H II region is  $0.04 \pm 0.07$  from Miralles et al. (1994) observations. This would give a flux of  $\sim 50$  mJy for the northern CH II region. Hence, the 1.28 GHz combined flux would be  $\sim 80$  mJy. The GMRT flux at 1.28 GHz is 103 mJy in a beam size of 30 arcsec that encompasses both the H II regions. This is a reasonably fair comparison considering the various uncertainties involved. Partitioning the flux in the same ratio, we estimate the flux due to the UCH II region at 1.28 GHz to be  $\sim 38$  and 65 mJy for CH II region.

Comeron & Torra (2001) showed for an ionization bounded H II region optically thin at frequency  $\nu$ , with an electron temperature of  $T_e \sim 10^4$  K, the distance may be given by

$$D(\text{kpc}) \approx 5.35 \times 10^{-3} \left[ \frac{\nu^{0.1}(\text{GHz}) S_\nu(J_y)}{\sum_{i=1}^N 10^{-1.26 H_{oi}}} \right]^{0.233}, \quad (1)$$

where  $S_\nu$  is the flux density in Jy at frequency  $\nu$  (in GHz).  $H_{oi}$  is the dereddened  $H$ -band magnitude;  $H_o = H$  (observed)  $- A_H$ , with  $A_H$ , the extinction in the  $H$  band.  $A_H$  may be estimated from the formula  $A_H = 0.11 + 2.87(H - K)$ , assuming the extinction law due to Rieke & Lebofsky (1985). The term 0.11 is to take care of the intrinsic colour for OB stars. Using this approximate formula, the GMRT radio fluxes and the combined  $H$ -band magnitudes of all the early B-type stars in the two H II regions in the Object 1 (Cluster 1), we obtain an average value of 4.8 kpc; and for the Object 2 (Cluster

2C), we get an average value of 7.3 kpc. The kinematic distance of 7.4 kpc was estimated by Wouterloot & Brand (1989) and adopted by Shepherd & Churchwell (1996). However, the distance problem that arises due to the excess photon flux (if placed nearer) may be circumvented due to the presence of more than one ionizing photon source. Our distance estimates are in good agreement with the value of 7.4 kpc adopted by earlier workers.

Using the GMRT fluxes, we then estimated the physical parameters such as electron density, emission measure and optical depth, following the standard work of Mezger & Henderson (1967), under the assumption of spherical H II region. Assuming the angular sizes of the two H II regions (UCH II region  $\sim 1.6$  arcsec and CH II region  $\sim 12$  arcsec) from Miralles et al. (1994), and a typical electron temperature of  $10^4$  K, we get the electron density  $N_e = 8.9 \times 10^3 \text{ cm}^{-3}$  and the emission measure  $\text{EM} = 6.6 \times 10^6 \text{ cm}^{-6} \text{ pc}$  for the UCH II region and  $N_e = 5.7 \times 10^2 \text{ cm}^{-3}$  and  $\text{EM} = 2.0 \times 10^5 \text{ cm}^{-6} \text{ pc}$  for the CH II region. If we adopted lower  $T_e$  (3300 K as derived by Miralles et al. 1994), we get the values of EM about 68 per cent of the values with  $T_e = 10^4$  K.

Having obtained the EM values, we can now calculate the optical depth values. For the GMRT fluxes, assuming  $T_e = 10^4$  K, we get  $\tau_c(1.28 \text{ GHz}) = 1.29$  for the UCH II region and 0.04 for the CH II region. If we adopt  $T_e = 3500$  K (see Miralles et al. 1994), we get  $\tau_c = 5.67$  for the UCH II region and 0.17 for the CH II region. This shows that the UCH II region is optically thick at 1.28 GHz (compare Miralles et al. 1994 for 4.9 and 14.9 GHz). This suggests that the H II region is not ionization bounded and hence the equation (1) may not be adequate for its distance estimation (for more discussion on this point, see Comeron & Torra 2001).

Similar calculations were performed for Object 2 (central cluster) also. We obtained a value of  $N_e = 2.8 \times 10^2 \text{ cm}^{-3}$  and  $\text{EM} = 1.2 \times 10^5 \text{ cm}^{-6} \text{ pc}$ , assuming the angular size of the source to be  $\sim 30$  arcsec. This yields the continuum (1.28 GHz) optical depth  $\tau_c = 0.023$  showing it is optically thin at this frequency. This could be the reason why this object was not detected in CS(2-1) line survey of Bronfman et al. (1996), since the line gets preferentially populated in denser regions. From the parameters derived from the radio continuum, it may be inferred that while the UCH II region is obviously the youngest, the CH II region in Cluster 1 is younger than the CH II region in Cluster 2C which, in turn, could be younger than Cluster 2N.

We then estimated the Lyman continuum photon fluxes from the  $N_e$  values and sizes of the H II regions (e.g. Smith 2004):  $2.3 \times 10^{47} \text{ s}^{-1}$  for the UCH II region and  $7.8 \times 10^{47} \text{ s}^{-1}$  for the CH II region in Object 1 and  $2.9 \times 10^{48} \text{ s}^{-1}$  for the CH II region in Cluster 2C (Object 2). If we consider the Lyman continuum fluxes for ZAMS stars of same spectral types as given in Tables 1–3, we obtain for Cluster 1 (adding the UCH II and CH II), a total of  $4.6 \times 10^{48} \text{ s}^{-1}$  and for Cluster 2C a total of  $1.8 \times 10^{48} \text{ s}^{-1}$  (from Thompson 1984). Our results are consistent with multiple early B-type or late O-type stars that account for the photon fluxes. Thus, within uncertainties, the derived radio properties support the NIR photometric results.

A similar analysis of radio continuum emission around Star A suggests that the emission region is optically thin ( $\tau_c = 0.006$ ) and the photon flux is consistent with a late O-type star.

#### 4.3 Association of the three clusters and the presence of Star A

It is clear from our infrared photometric study as well as the previous radio studies that the two *IRAS* sources are most likely associated with each other, probably belonging to the same parent molecular

cloud. One can note in Fig. 5 that the colours of YSOs in the three clusters are nearly the same, although those in Cluster 1 are slightly redder in comparison. Age estimates (Palla & Stahler 2000) from the CMD of absolute  $J$  versus  $J - H$  showed that all the three clusters have similar ages with all the moderately massive stars being close to ZAMS. It should be mentioned here that while the two *IRAS* sources are nearly at the same kinematic distance (from published radio observations of Wouterloot & Brand 1989; Carral et al. 1999), attributing them to the same molecular cloud should reconcile with a large velocity gradient across the cloud (from the published CO line data of Yang et al. 2002).

What is more intriguing, however, is the presence of Star A between the two sources (at a projected separation of  $\sim 10$  pc from either, assuming the same distance for the Clusters and Star A) and the indication of its possible association with the three clusters as can be seen from the MSX *A*-band image (Fig. 6). We will examine the possibility for Star A to have initiated the star formation in the three clusters.

It was proposed and subsequently evidences were shown by several authors that young massive stars can trigger star formation in the surrounding interstellar medium, either by their expanding H II regions sweeping up material that may collapse by a gravitational perturbation (Elmegreen & Lada 1977) or by the radiation-driven collapse of already present clumpy matter (Lefloch, Lazareff & Castets 1994; Karr & Martin 2003; Zinnecker & Yorke 2007, and the references therein).

The enigmatic single star (Star A) located in the region between the two *IRAS* sources suggests that this star being very massive, its winds/radiation might have prevented any further star formation in the near vicinity. But it is possible that farther away, the winds/radiation originated from this star might have triggered the intermediate to moderately high-mass star formation in the three clusters flanking it. But we need to reconcile with the large extinction that the star suffers.

The large extinction may be attributed to an accretion disc. Being a massive star, it is possible that the winds and energetic radiation are switched on (upon entering the ZAMS stage), even before accretion phase ceases. It is also possible that the winds and radiation from the star could escape through the polar regions and interact with the surrounding matter. The formation time-scale for a massive star is about  $5 \times 10^5$  yr; the time-scales for the accretion disc to evaporate following the onset of energetic radiation and winds from the PMS star are also of the same order (see e.g. Churchwell 2002; McKee & Ostriker 2007).

However, the non-detection of Star A in the far-IR (beyond  $25 \mu\text{m}$ ) by *IRAS* (or *COBE*) casts doubts on being massive as argued by us and hence in the triggering scenario. Alternatively then the Star A could be a nearby foreground star in that case its spectral type would be that of an intermediate low-mass PMS star suffering high extinction.

Further deeper observations are required on the entire molecular cloud complex using an appropriate molecular tracer in order to resolve both these issues, viz. the large-velocity gradient across the cloud and the nature of Star A.

## 5 CONCLUSIONS

The important conclusions of this work are the following.

(i) Seeing limited NIR photometry was made on two massive star-forming regions IRAS 21413+5442 and IRAS 21407+5441 using UKIRT facility. A radio continuum mapping of the two

regions was also done using GMRT facility in the 1.28-GHz band.

(ii) Several embedded early B-type stars are detected in both IRAS 21413+5442 (Cluster 1) and IRAS 21407+5441 (Clusters 2C and 2N). Several PMS stars are detected only in *H* and *K* bands having large  $H - K$  colours (red objects) in all the three clusters. One such red object in Cluster 1, possibly a late O-type star is located very close to the centre of the CO outflows in IRAS 21413+5442. A new CHII region was identified in the Cluster 2C which is powered by early B-type or late O-type stars.

(iii) Our infrared photometry and the radio map along with the MSX *A*-band image indicate that the two *IRAS* sources are associated with each other. A highly obscured massive (O4 or earlier) star is shown to be present in the region between the two *IRAS* sources. It is conjectured that this single massive star might have triggered the star formation in the clusters. Further investigation is needed to establish this hypothesis beyond doubt.

(iv) The radio continuum observation at 1.28 GHz confirms the earlier results that the UCHII region in IRAS 21413+5442 is optically thick with the spectral index 1.0. The radio properties seem to support the NIR photometric results.

## ACKNOWLEDGMENTS

We thank the anonymous referee for a stimulating report that helped in improving the original version of the manuscript. This research was supported by the Department of Space, Government of India. MSNK is supported by the project PTDC/CTE-AST/65971/2006 approved by the Portuguese National Science Foundation (PCT). We thank the staff of GMRT (NCRA-TIFR) at Khodad, Central India for their help in obtaining the radio observations. We also thank the staff of UKIRT, Hawaii for observational time and help. This publication makes use of data products from the 2MASS, which is a joint project of the University of Massachusetts and the IPAC/California Institute of Technology, funded by NASA and NSF. This research has also made use of the data products from the MSX, NASA/IPAC Infrared Science Archive, which is operated by the Jet Propulsion Laboratory, California Institute of Technology, under contract with NASA. The use of *DUSTY* code is thankfully acknowledged.

## REFERENCES

- Bessell M. S., Brett J. M., 1988, *PASP*, 100, 1134
- Beuther H., Schilke T. K., Sridharan T. K., Menten K. M., Walmsley C. M., Wyrowski F., 2002, *A&A*, 383, 892
- Blum R. D., Daminieli A., Conti P. S., 2001, *AJ*, 121, 3149
- Bronfman L., Nyman L.-A., May J., 1996, *A&AS*, 115, 81
- Campbell B., Persson S. E., Matthews K., 1989, *AJ*, 98, 643
- Carral P., Kurtz S., Rodriguez L. F., Marti J., Lizano S., Osorio M., 1999, *Rev. Mex. Astron. Astrofis.*, 35, 97
- Churchwell E., 2002, *ARA&A*, 40, 27
- Comeron F., Torra J., 2001, *A&A*, 375, 539
- Elmegreen B. G., Lada C. J., 1977, *ApJ*, 214, 725
- Hawarden T. G., Leggett S. K., Letawsky M. B., Ballantyne D. R., Casali M. M., 2001, *MNRAS*, 325, 563
- Hunt L. K., Mannucci F., Test L., Migliorini S., Stanga R. M., Baffa C., Lisi F., Vanzi L., 1998, *AJ*, 115, 2594
- Ishii M., Nagata T., Sato S., Watanabe M., Yao Y., 1998, *AJ*, 116, 868
- Ishii M., Hirao T., Nagashima C., Nagata T., Sato S., 2002, *AJ*, 124, 430
- Ivezic Z., Nenkova M., Elitzur M., 1999, User Manual for *DUSTY*, University of Kentucky Internal Report (<http://www.pa.uky.edu/moshe/dusty>)
- Karr J. L., Martin P. G., 2003, *ApJ*, 595, 900

- Kumar M. S. N., Keto E., Clerkin E., 2006, *A&A*, 449, 1033  
Lada C., 1985, *ARA&A*, 23, 267  
Lada C., Adams F. C., 1992, *ApJ*, 393, 278  
Lefloch B., Lazareff B., Castets A., 1997, *A&A*, 324, 249  
McKee C. F., Ostriker E. C., 2007, *ARA&A*, 45, 565  
Meyer M. R., Calvet N., Hillenbrand L. A., 1997, *AJ*, 114, 288  
Mezger P. G., Henderson A. P., 1967, *ApJ*, 147, 471  
Miralles M. P., Rodriguez L. F., Scalise E., 1994, *ApJS*, 92, 173  
Palla F., Stahler S. W., 2000, *ApJ*, 540, 255  
Price S. D., Egan M. P., Carey S. J., Mizuno D. R., Kuchar T. A., 2001, *AJ*, 121, 2819  
Rieke G. H., Lebofsky M. J., 1985, *ApJ*, 288, 618  
Scheffler H., Elsasser H., 1988, *Physics of the Galaxy and Interstellar Matter*. Springer-Verlag, Berlin  
Shepherd D. S., Churchwell E., 1996, *ApJ*, 472, 225  
Smith M. D., 2004, *The Origin of Stars*. Imperial College Press, London  
Swarup G., Ananthakrishnan S., Kapahi V. K., Rao A. P., Subrahmanya C. R., Kulkarni V. K., 1991, *Curr. Sci.*, 60, 95  
Thompson R. I., 1984, *ApJ*, 283, 165  
Thompson R. I., Corbin M. R., Young E., Schneider G., 1998, *ApJ*, 492, L177  
Weintraub D. A., Kastner J. H., 1996, *ApJ*, 458, 670  
Wood D. O. S., Churchwell E., 1989, *ApJS*, 69, 831  
Wouterloot J. G. A., Brand J., 1989, *A&AS*, 80, 149  
Wouterloot J. G. A., Brand J., Burton W. B., Kwee K. K., 1990, *A&A*, 230, 21  
Yang J., Jiang Z., Wang M., Ju B., Wang H., 2002, *ApJS*, 141, 157  
Zinnecker H., Yorke H. W., 2007, *ARA&A*, 45, 481

This paper has been typeset from a  $\text{\TeX}/\text{\LaTeX}$  file prepared by the author.